Available online at www.sciencedirect.com
SCIENCE DIRECT®
Journal of Sound and Vibration 274 (2004) 137–161
JOURNAL OF SOUND AND VIBRATION
www.elsevier.com/locate/jsvi

Identifying the foundation stiffness of a partially embedded post from vibration measurements

T.P. Waters*, M.J. Brennan, S. Sasananan

Institute of Sound and Vibration Research, University of Southampton, Highfield, Southampton SO17 1BJ, UK

Received 16 January 2003; accepted 15 May 2003

Abstract

Foundations of posts such as lighting columns can suffer damage or deteriorate over time, rendering the post unsafe. Quick, inexpensive and non-intrusive measurement procedures are required to monitor periodically their structural integrity. This paper investigates the behaviour of beam-like structures with a view to identifying a suitable monitoring technique for post foundations. In this initial study a lighting column is modelled as a uniform rigid beam that is constrained by collocated equivalent translational and rotational springs. Expressions are derived for the equivalent spring constants as functions of foundation profile and depth.

Modal and static responses are presented as functions of foundation properties. The inverse problem of identifying the foundation stiffnesses from response measurements is discussed. A simple method is proposed based on quasi-static stiffness measurements obtained from impact tests. The method is validated using measurements of a laboratory scale structure.

1. Introduction

Engineering structures are designed to withstand in excess of the dynamic and static loads they may be expected to experience during their life spans. However, damage inflicted on a structure or deterioration due to age or misuse will reduce a structure's load-bearing capability. Non-destructive testing (NDT) methods are required to test periodically or monitor continuously the integrity of safety-critical structures. The considerable research effort that is directed into this activity reflects the enormous potential and actual losses that can be attributed to structural failure.

*Corresponding author. Tel.: +44-23-8059-4979; fax: +44-23-8059-3190.
E-mail address: tpw@isvr.soton.ac.uk (T.P. Waters).

0022-460X/$ - see front matter
doi:10.1016/j.jsv.2003.05.011

Lighting columns, whilst modest in many ways compared to some large and costly civil and aerospace structures, pose a real threat to personal injury [1]. The challenge of developing an NDT technique for lighting columns differs from aircraft and highway bridges, for example, due to their abundance and lower unit value. Any assessment technique must be simple, inexpensive, quick to carry out and preferably requiring minimal specialist skills. Fortunately, lighting columns are comparatively simple structures that are conducive to simple and physically interpretable analysis and measurement.

Vibration response as an indicator of structural change has been advocated for many years. Modal parameters (natural frequencies [2,3], mode shapes [4,5] and loss factors [6]) are popular because they are global properties of the structure, so can detect the existence of damage from sensors far removed from the damaged area. However, modal parameters are less able to provide localised information such as the damage site [7]. In practice, changes in modal parameters due to damage can be either immeasurably small or indistinguishable from non-damage events such as environmental changes, load conditions, and so on [8,9]. At the other end of the frequency spectrum ultrasound techniques give localised information close to the measurement location but are insensitive to damage elsewhere due to signal attenuation. Comprehensive reviews of NDT methods [10] and vibration based techniques in particular [11,12] are available in the literature.

To the best of the authors' knowledge there are no publications relating specifically to damage assessment of lighting column foundations. However, a number of researchers have considered similarly constrained one-dimensional structures. Pines investigated the detection of fungal decay in wooden telegraph poles by measuring the reflection coefficient of axial waves [13]. Assessment of the internal decay of living trees has been attempted from natural frequencies of circumferential modes [14] and impulse response functions [15]. Choy et al. used changes in natural frequencies to locate damage in a beam such as a pavement or rail track resting on an elastic foundation [16]. Purekar and Pines used dereverberation techniques to estimate flexural wave propagation from transfer functions of rotor blades [17].

In this paper a lighting column is modelled as a rigid beam which is partially embedded in an elastic foundation. The analysis may be extended to include flexibility of the beam but is beyond the scope of this initial study. Damage is assumed to occur only in the foundation causing changes in the equivalent stiffness in translation and rotation at the constrained end of the beam. The sensitivity of the beam's modal and static responses to foundation parameters is presented. A simple technique for identifying foundation stiffnesses from quasi-static stiffness measurements is presented and validated through laboratory experiments.

2. Discrete spring model of foundation

2.1. The model

The simplest and most suitable first approximation to a partially embedded post is a rigid beam constrained at one end by translational and rotational springs, as shown in Fig. 1. The beam is taken to be uniform (which determines the rigid body inertia of the system) and the springs are assumed to be linear with equivalent translational and rotational stiffnesses of k_t and k_r.

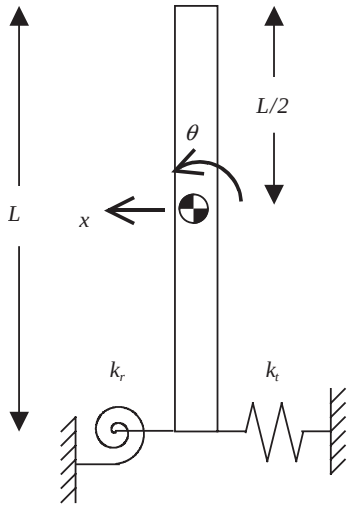

Fig. 1. Rigid beam constrained at one end by translational and rotational springs.

Deterioration of the foundation can be expected to affect both k_t and k_r in general. The special case when both quantities change in the same proportions is trivial for a rigid beam and corresponds to a simple scaling of the system. Instead, only disproportionate changes between k_t and k_r are considered and the normalised rotational stiffness is defined as

$$\gamma = \frac{k_r}{k_t L^2}, \tag{1}$$

where L is the entire length of the beam. This parameter is used in the following analyses in order to non-dimensionalise the equations of motion.

2.2. Modal response

Assuming rigid body motion in one plane, the simple model shown in Fig. 1 has two degrees of freedom (DOFs). Taking $\{x, L\theta\}^{\mathrm{T}}$ as the DOF variables, where x is the translational displacement at the centre of mass and θ is the rotational displacement, then either equilibrium of forces and moments or Lagrange's equations can be used to derive the following stiffness and mass matrices:

$$\mathbf{K} = k_t \begin{bmatrix} 1 & -\frac{1}{2} \\ -\frac{1}{2} & \frac{1}{4} + \gamma \end{bmatrix}, \quad \mathbf{M} = m \begin{bmatrix} 1 & 0 \\ 0 & \frac{1}{12} \end{bmatrix}, \tag{2}$$

where m is the mass of the beam. Fig. 2 shows the two natural frequencies as a function of normalised rotational stiffness, γ. The frequencies have been normalised by $\sqrt{k_t/m}$. The nodal points of the corresponding mode shapes are shown in Fig. 3.

For small values of γ (low rotational stiffness), the natural frequencies and mode shapes show asymptotic behaviours. The lower frequency mode is proportional to the square root of rotational stiffness and is a pure pitching motion about the constrained end. Consequently, only the rotational spring deforms significantly and so the system can be represented by a simply supported beam with an associated equivalent inertia of $\frac{1}{3}mL^2$, as shown in the bottom left

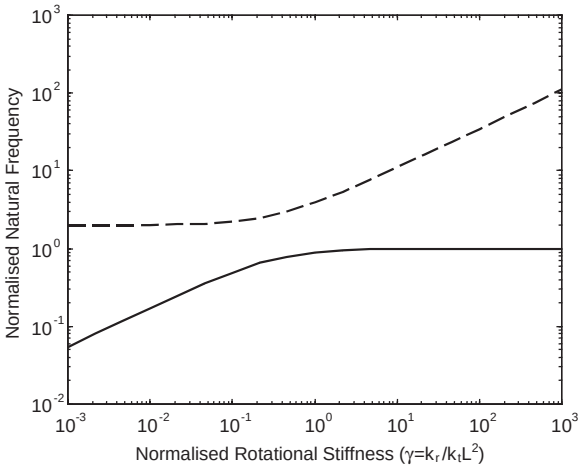

Fig. 2. Normalised natural frequencies of rigid beam constrained at one end as a function of normalised rotational stiffness.

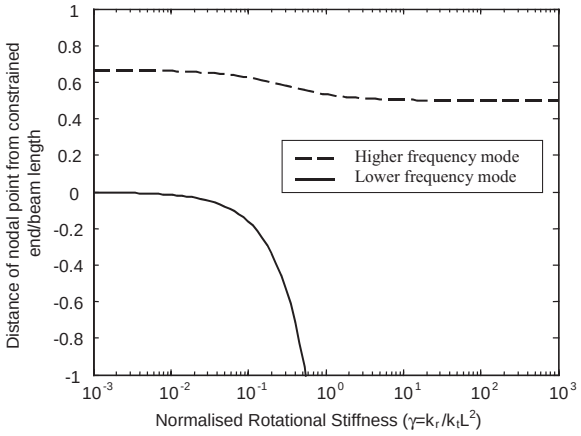

Fig. 3. Mode shapes of rigid beam constrained at one end as a function of normalised rotational stiffness.

schematic of Fig. 4. Conversely, the frequency of the higher mode is independent of rotational stiffness. The mode shape is a pitching motion with a nodal point at $\frac{2}{3}L$ such that the restoring moment is dominated by the translational spring. The mode can be represented simply by the equivalent mass of the beam at its end, namely $m/4$, supported by the translational spring, as shown schematically in the top left corner of Fig. 4.

For large values of γ different asymptotic behaviours are observed. The lower frequency mode becomes independent of rotational stiffness which is now large enough to suppress any significant rotation. The nodal point tends to minus infinity indicating a pure sidewards motion. The system can be represented by a sliding condition as shown in the bottom right schematic in Fig. 4. The natural frequency is determined by the translational spring constant and the overall mass of the beam, m. In the higher frequency mode, the translational spring becomes negligible and the beam

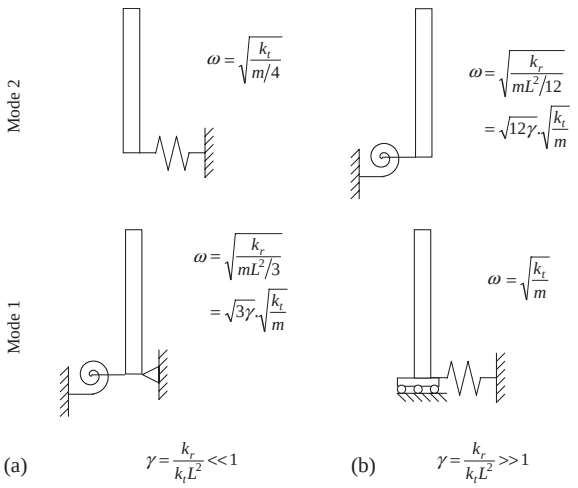

Fig. 4. Approximate representation of modes of constrained beam for (a) small; and (b) large normalised rotational stiffness.

is constrained only in rotation, see Fig. 4 (upper right). Consequently, the beam pitches about its centre of mass. The frequency is proportional to the square root of rotational stiffness and inversely proportional to the square root of the inertia about the beam's midpoint, namely $\frac{1}{12}mL^2$.

Between these distinct regions of dynamic behaviour is a transition region where these idealised representations of the system break down. It is only in this region that the mode shapes are sensitive to changes in rotational stiffness. Note also that the natural frequencies do not cross in the transition from one region to the other. This is consistent with the fully populated form of the stiffness matrix in Eq. (2) which prevents repeated roots.

It is not possible to ascertain from this analysis which region of modal behaviour typifies actual lighting columns. However, it is clear that if either region prevails in practice then one natural frequency is proportional to the square root of the translational stiffness and the other is proportional to the square root of the rotational stiffness. It can be concluded that the natural frequencies are only moderately sensitive to changes in the stiffnesses of the foundation.

2.3. Static response

This section considers the static response of the rigid beam shown in Fig. 1. Assume that we may measure—either by static or dynamic means—the translational response X_s at one point on the beam due to a static force F at another point. The sensor and force are located at distances l_s and l_f, respectively, from the constrained end. Then the static response can be related to the translational and rotational spring deflections, x and θ, as follows:

$$X_s = x + l_s\theta. \tag{3}$$

Introducing equilibrium of forces and moments this can be rewritten as

$$X_s = \frac{F}{k_t} + \frac{l_s l_f F}{k_r}. \tag{4}$$

The static stiffness is given by the static force per unit displacement,

$$K = \frac{1}{\dfrac{1}{k_t} + \dfrac{1}{k_r/l_s l_f}}. \tag{5}$$

The system is equivalent to two springs of stiffness k_t and $k_r/l_s l_f$ in series. When either the sensor or force position is at the constrained end of the beam then only the translational spring is seen and, in theory, its stiffness coefficient can be determined by a single measurement. Note also from Eq. (5) that the static stiffness is proportional (equal) to k_t in this region. Therefore, static stiffness is a more sensitive measure of deterioration in translational stiffness than are natural frequencies (see Section 2.2). However, static stiffness measured here will not observe any defect in the foundation that affects only the rotational stiffness.

As the force and response positions move towards the free end of the beam then the contribution of the foundation's rotational stiffness to the static stiffness increases. In practice, the force and sensor locations are limited by the height of the post ($l_f, l_s \leqslant L$), but in theory at least the static stiffness will become dominated by and proportional to the rotational spring stiffness as $l_s l_f$ becomes (perhaps unfeasibly) large. The static stiffness, if measured here, is insensitive to changes in the foundation's translational stiffness.

The effect on static stiffness of the measurement position and the foundation properties is seen more clearly by non-dimensionalising Eq. (5) as follows:

$$\frac{K}{k_t} = \frac{1}{1 + 1/(\gamma/\beta^2)}, \tag{6}$$

where $\gamma = k_r/k_t L^2$ is the normalised rotational stiffness parameter defined earlier, and

$$\beta = \frac{1}{L}\sqrt{l_s l_f}. \tag{7}$$

The parameter β is the geometric mean of the force and response locations when expressed as a fraction of the beam length, and is bounded between 0 and 1. In the case of a point measurement β is simply the (normalised) distance of the measurement from the constrained end.

Fig. 5 shows the normalised static stiffness given by Eq. (6) as a function of γ/β^2. An increasing abscissa corresponds to an increase in rotational stiffness or a movement lower down the post of the force and/or sensor.

The dominance of the response by one or other of the two springs in series is characterised by the curve's asymptotes. When $\gamma/\beta^2 \ll 1$ the static stiffness is controlled by the rotational spring and is therefore dependent on the measurement location. When $\gamma/\beta^2 \gg 1$ the static stiffness is dominated by deformation of the translational spring which is not affected by the force position.

One wishes to conclude from Fig. 5 whether static stiffness measurements may be used to observe the translational and/or rotational stiffness of a foundation. However, it is not possible to draw such a conclusion without first establishing bounds on the parameter γ/β^2. In practice, the entire range of $0 \leqslant \beta^2 \leqslant 1$ may not be achievable, either because small values require measurements to be taken below ground level or because large values require measurements at impracticable heights. Furthermore, the preceding analysis provides no insight into what values of normalised

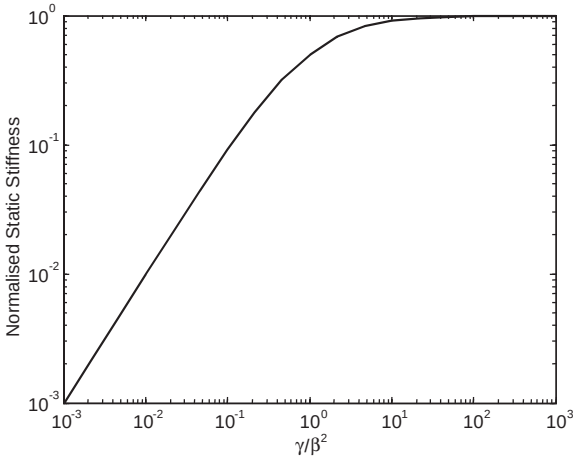

Fig. 5. Static response of constrained beam as a function of γ/β^2 (γ is the normalised rotational stiffness; β is the geometric mean of the force and response positions normalised by beam length).

rotational stiffness, γ, are typical or achievable. The next section explores an alternative model of the foundation, the analysis of which will resolve this issue.

3. Continuous elastic model of foundation

3.1. General model

The model developed in the previous section is conceptually simple and, by appropriate non-dimensionalisation, is useful in characterising in general terms the response of a constrained rigid beam. Distinct regions of behaviour were observed in both the modal and static response that can be related directly to the physical parameters of the system. The normalised rotational stiffness, γ, which defines the relationship between the rotational and translational stiffnesses, was found to be the key parameter that governs which response characteristic prevails.

The model developed in this section explores the relationship between rotational and translational stiffness of a continuous elastic foundation of depth l. Typical and upper bound values for γ are obtained thereby providing insight into the feasibility of detecting damage via modal or static response measurements.

Fig. 6(a) shows a rigid beam constrained along length l of one end by an elastic medium. The foundation is taken to be axisymmetric so that the equivalent stiffness due to compression of the foundation medium is the same in any direction radial to the post. Shear effects are neglected. A strip-wise approach is adopted whereby the stiffness per unit length of the foundation is denoted by $w(z)$, where z is the distance from the constrained end of the beam. The inertia and damping of the elastic medium are neglected. There exists an elastic centre at which the translational and rotational motions of the beam are not coupled by the elastic foundation. The continuous model can be represented by discrete translational and rotational springs of equivalent stiffness collocated at the elastic centre, as shown in Fig. 6(b).

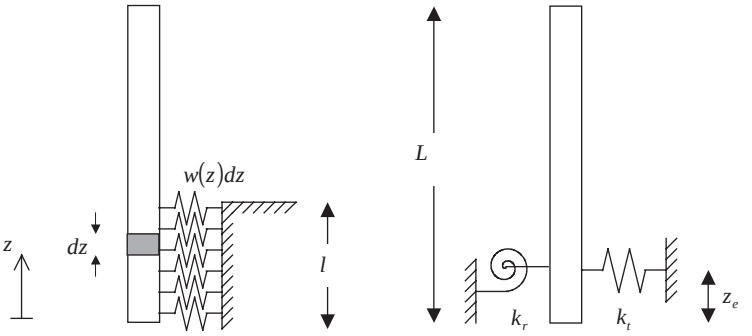

(a) Continuous elastic foundation (b) Discrete equivalent foundation

Fig. 6. Model of distributed foundation.

Denoting the location of the elastic centre as z_e, then by definition a sidewards translation, X_e, at this point will produce zero spring moment. Taking moments about the elastic centre gives

$$\int_0^l w(z)X_e(z - z_e)\,\mathrm{d}z = 0. \tag{8}$$

Therefore, the elastic centre can be found from evaluating

$$z_e = \int_0^l w(z)z\,\mathrm{d}z \Big/ \int_0^l w(z)\,\mathrm{d}z. \tag{9}$$

The equivalent stiffness of translational and rotational springs placed at the elastic centre can be found by equilibrium of forces and moments to be:

$$k_t = \int_0^l w(z)\,\mathrm{d}z, \quad k_r = \int_0^l w(z)(z - z_e)^2\,\mathrm{d}z. \tag{10}$$

3.2. Specific foundation models

The relations developed in the preceding section are valid for any stiffness profile, $w(z)$, within the assumptions of the model. In this paper, two special cases are considered: a uniform distribution, and the distribution that maximises rotational stiffness.

3.2.1. Uniform stiffness profile

An algebraically convenient—and perhaps not entirely inappropriate stiffness profile is one that is constant with depth, i.e., $w(z)$ is a constant. Then Eq. (9) can be evaluated simply to confirm the intuitively obvious result that the elastic centre occurs at the mid-depth of the foundation, $z_e = l/2$.

Hence, the equivalent translational and rotational stiffnesses can be evaluated from Eq. (10):

$$k_t = wl, \quad k_r = \tfrac{1}{12}wl^3. \tag{11}$$

Combining these expressions gives

$$k_r = \tfrac{1}{12} k_t l^2. \tag{12}$$

Eq. (12) shows that the rotational stiffness is proportional to the translational stiffness and the square of the foundation depth. The constant of proportionality, p say, is a function of the foundation profile and is given by $p = \frac{1}{12}$ when the profile is uniform.

It is convenient to express Eq. (12) in the following form:

$$\frac{k_r}{k_t L^2} = \tfrac{1}{12} \hat{l}^2, \tag{13}$$

where $\hat{l} = l/L$ represents the proportion of the beam embedded in the foundation.

The parameter $k_r/k_t L^2$ in Eq. (13) is the normalised rotational stiffness, γ, defined in Section 2, although the equivalent springs are now collocated at the elastic centre rather than the constrained end of the beam.

Now that a relationship between rotational and translational stiffness has been established it is possible to consider the modal and static response of the model as a function of normalised foundation depth, $\hat{l}$, which is bounded between 0 and 1. First, it is convenient to establish an upper bound on the foundation profile constant, p.

3.2.2. Maximum rotational stiffness profile

Suppose that the total equivalent translational stiffness of the foundation is fixed, but that the distribution can be varied. Then the rotational stiffness is at a maximum when the spring distribution delivers point forces at either end of the foundation. This situation is depicted in Fig. 7. In terms of the continuous foundation model of Section 3.1 the stiffness per unit length of

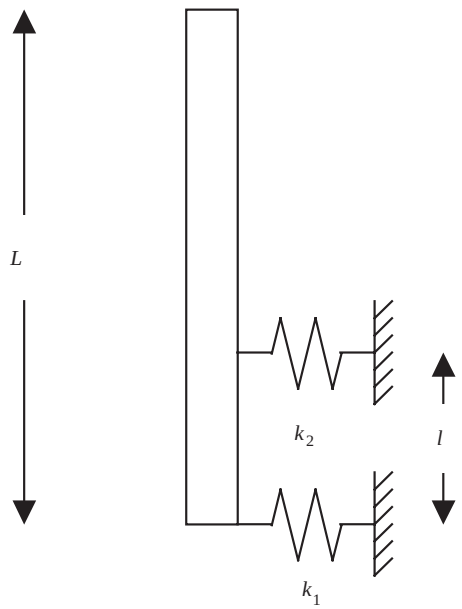

Fig. 7. Foundation profile that maximises rotational stiffness.

the foundation becomes:

$$w(z) = \delta(0)k_1 + \delta(l)k_2 \tag{14}$$

where δ denotes the Dirac delta function and k_1 and k_2 are the discrete spring stiffnesses at either end of the foundation. Evaluation of the equivalent stiffnesses and the elastic centre is possible by substituting $w(z)$ into Eqs. (9) and (10), but unnecessarily cumbersome. Returning to first principles the following expressions can be derived more simply:

$$z_e = \frac{1}{1+a}l \tag{15}$$

and

$$k_t = k_1 + k_2, \quad k_r = \frac{a}{(1+a)^2}l^2 k_t, \tag{16a, b}$$

where $a = k_1/k_2$. The normalised rotational stiffness, γ, follows from Eq. (16b)

$$\gamma = \frac{k_r}{k_t L^2} = \hat{l}^2 \frac{a}{(1+a)^2}, \tag{17}$$

where $\hat{l} = l/L$ represents the proportion of the beam embedded in the foundation, as defined earlier. The function $a/(1+a)^2$ appearing in the normalised rotational stiffness is the foundation profile constant, p, and tends to zero when either $k_1 \to 0$ or $k_2 \to 0$. Physically, these two cases correspond to a single discrete spring at only one of the ends of the foundation. In either case one would expect the beam to be unconstrained in rotation.

It can also be shown that the foundation profile constant $a/(1+a)^2$ attains a maximum value of $\frac{1}{4}$ when $a = 1$, i.e., when the springs are equal in stiffness. This idealised case is useful insofar as it represents an upper bound on the normalised rotational stiffness,

$$\gamma = \frac{k_r}{k_t L^2} \leqslant \tfrac{1}{4}\hat{l}^2. \tag{18}$$

By comparing Eqs. (13) and (18) it can be seen that a uniform stiffness distribution gives one third of the maximum achievable rotational stiffness.

Besides defining a bound on the achievable rotational stiffness from a continuous elastic foundation, this somewhat unrealistic foundation profile is realisable, repeatable and controllable in a laboratory and therefore ideal for the purposes of experimental validation. The design and measurement of a rig featuring discrete translational springs with variable separation is the subject of Section 5.

3.3. Modal response

This section considers the free vibration of the system shown in Fig. 6(b). Recall that this system models the continuous elastic foundation depicted in Fig. 6(a) by discrete translational and rotational springs at the elastic centre.

The intention here is to evaluate the sensitivity of the modal parameters to changes in foundation profile, or equivalently, the ratio of rotational to translational stiffness. (The case when rotational and translational stiffnesses change in proportion to one another is trivial in that both frequencies change with the square root of stiffness and the mode shapes are unaffected.)

Taking $\{x, L\theta\}^{\mathrm{T}}$ as the DOF variables, where x is the translational displacement at the centre of mass and θ is the rotational displacement, then the mass and stiffness matrices can be derived by equilibrium or Lagrange's equations giving

$$\mathbf{K} = k_t \begin{bmatrix} 1 & -\frac{1}{2}(1-\hat{l}) \\ -\frac{1}{2}(1-\hat{l}) & \frac{1}{4}(1-\hat{l})^2 + \gamma \end{bmatrix}, \quad \mathbf{M} = m \begin{bmatrix} 1 & 0 \\ 0 & \frac{1}{12} \end{bmatrix}, \tag{19}$$

where the equivalent stiffness of the translational spring, k_t, is a function of foundation depth and is given by Eq. (10).

The modal parameters for the general system described by Eq. (19) are presented for the two foundation profiles discussed in Section 3.2. The uniform profile and the discrete translational spring profile give rise to a normalised rotational stiffness of $\frac{1}{12}\hat{l}^2$ and $\frac{1}{4}\hat{l}^2$ respectively.

Fig. 8 shows the natural frequencies of the two modes as a function of foundation depth. The frequencies have been normalised by the heave frequency of the beam when fully buried in a uniform foundation, i.e., $\sqrt{wL/m}$.

Following the discussion in Section 2.2 for the simple beam model constrained at its end, and recalling that γ is proportional to $\hat{l}^2$, one might have expected Fig. 8 to have shown two distinct regions of modal behaviour. The first of those regions is apparent where the lower frequency mode is controlled by the rotational spring and the higher mode is controlled by the translational spring. Note that the translational stiffness is proportional to foundation depth so the frequencies increase with $\hat{l}^{3/2}$ and $\hat{l}^{1/2}$ respectively. The second region, where the lower frequency mode is controlled by the translational spring, does not arise although transition towards this behaviour is evident when the beam is predominantly buried.

The effect of foundation profile for a given translational stiffness is clearly seen in Fig. 8. The frequency of the lower mode is increased by a factor of about $\sqrt{3}$ for the threefold difference in rotational stiffness between the two foundation profiles. The higher frequency mode is largely unaffected by foundation profile.

Of academic interest is when the post is fully buried ($\hat{l} = 1$). The stiffness matrix in Eq. (19) becomes diagonal giving rise to an uncoupled system. In the case of a uniform foundation the

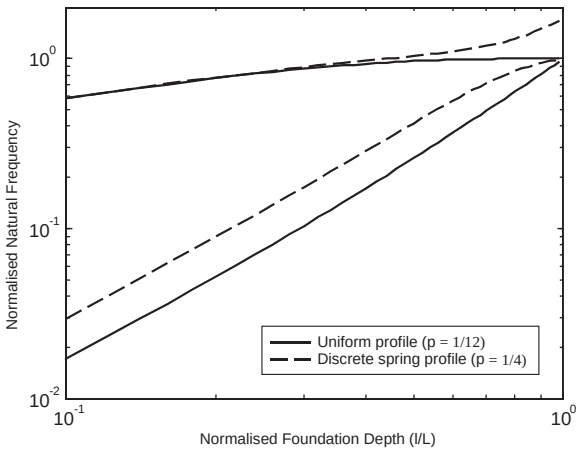

Fig. 8. Natural frequencies of beam mounted in elastic foundation of varying depth.

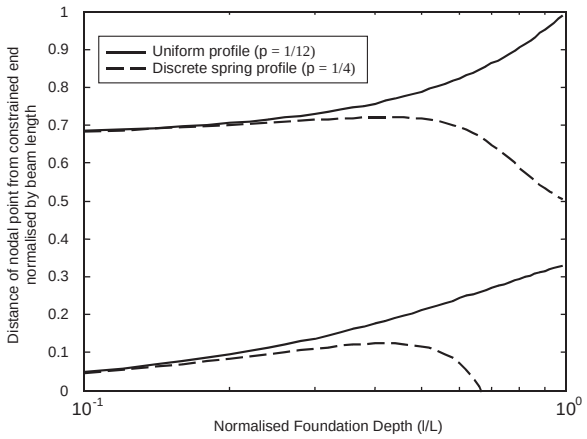

Fig. 9. Nodal points of modes of beam mounted in elastic foundation of varying depth.

roots are repeated owing to a coincidental factor of $L^2/12$ between mass and inertia and also translational and rotational stiffness.

Fig. 9 shows the location of the nodal points of the mode shapes as a function of foundation depth. For shallow foundations ($\hat{l}<0.3$, say) the mode shapes are similar for the two different foundation profiles. The lower frequency mode pitches about a point close to the constrained end of the beam and the higher frequency mode pitches at about two third of the beam's length. This result is consistent with the simpler model discussed in Section 2 of a beam with point constraints at its end.

For deeper foundations ($\hat{l}>0.3$) the difference in rotational stiffness of the two foundation profiles becomes apparent. In the case of the uniform foundation the nodal points of both modes continue to migrate away from the constrained end of the beam. In the limit when the beam is fully buried the mode shapes pitch about the free end and one-third of the beam's length. In the case of the point stiffness foundation the locations of the nodal points reach a maximum at about $\hat{l}=0.45$. As $\hat{l}\to 1$, one mode transforms into a pitching motion about the midpoint of the beam and the nodal point of the other tends to negative infinity indicating a pure heave mode.

If the three-fold difference in rotational stiffness between the two foundations were considered realistic of actual degradation or damage one might conclude that when $\hat{l}>0.3$ changes in foundation profile may be monitored by tracking nodal points. However, for more moderate changes in rotational stiffness this approach may be discarded unless the post is predominantly underground.

3.4. Static response

Section 2.3 considered the static response of a rigid beam constrained at one end by equivalent translational and rotational springs. The continuous elastic foundation differs from this idealised case only in that the equivalent springs must be located at the elastic centre rather than the end of

the beam. The static stiffness is again given by

$$K = \frac{1}{1/k_t + 1/(k_r/l_s l_f)} \tag{20}$$

although the sensor and force locations, l_s and l_f, are now measured from the elastic centre. Substituting for $k_r = pk_t l^2$ where p is the foundation profile constant gives

$$K = k_t \frac{1}{1 + l_s l_f / pl^2}. \tag{21}$$

It is convenient to define h as the geometric mean of the sensor and force locations normalised by the foundation depth, i.e.,

$$h = \frac{1}{l}\sqrt{l_s l_f}. \tag{22}$$

In the specific case when the response and input force are at the same point then h is the distance of the point measurement above the elastic centre expressed as a multiple of foundation depth. The normalised static stiffness is given by

$$\frac{K}{k_t} = \frac{1}{1 + h^2/p} \tag{23}$$

which can be thought of as two springs in series of normalised stiffness p/h^2 and unity. The individual spring constants and their sum in series are plotted as functions of h in Fig. 10. Results are presented for the two specific foundations considered in Section 3.2: (a) discrete springs at the

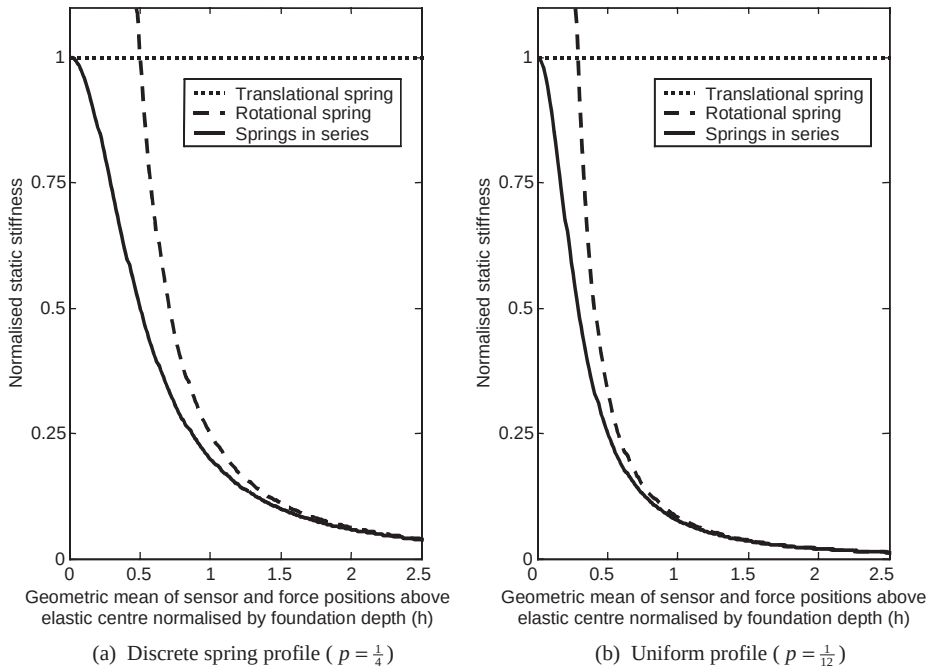

(a) Discrete spring profile ($p = \frac{1}{4}$) (b) Uniform profile ($p = \frac{1}{12}$)

Fig. 10. Static stiffness of beam mounted in elastic foundation as a function of measurement location.

bottom and top of the foundation ($p = \frac{1}{4}$), and (b) a uniform stiffness distribution ($p = \frac{1}{12}$). In both cases the elastic centre is at the mid-depth of the foundation so a point measurement at ground level corresponds to a value of $h = \frac{1}{2}$.

Fig. 10 shows that if it were practical to conduct a point measurement underground at the elastic centre ($h = 0$) then only the translational spring would be apparent. However, non-intrusive measurements can only be taken above ground level ($h \geqslant \frac{1}{2}$) where the rotational spring contributes significantly to the static stiffness. The translational spring will be most apparent for foundations profiles with a high rotational stiffness, the discrete translational spring profile defining the upper bound. In this limiting case, shown in Fig. 10(a), deformation of the rotational spring accounts for 50% of the translational response at ground level and dominates the response when $h \geqslant 1$ to $1\frac{1}{2}$. Fig. 10(b) illustrates that for a uniform foundation profile the static response at any point on the exposed length of the beam is controlled by the rotational spring. The rotational stiffness may be estimated (under-estimated) from a single measurement towards the free end of the beam.

4. Identifying foundation stiffnesses from dynamic measurements

4.1. Modal or static response?

Section 3 considered the behaviour of a rigid lighting column embedded in an elastic foundation and discussed the suitability of modal and static response measurements for identifying foundation stiffnesses. It has been shown that the lower and higher frequency rigid body modes are controlled by the rotational and translational foundation stiffnesses, respectively, over almost the full range of foundation depths. The natural frequencies can be expected to vary with the square root of deterioration in foundation stiffness.

It was also established that the static stiffness of the system is controlled by two springs of stiffness k_t and $k_r/l_s l_f$ in series where l_s and l_f are the sensor and force locations. In theory, two measurement positions may be chosen such that first the translational spring and then the rotational spring dominates enabling identification of each coefficient individually. Furthermore, static stiffness measurements are proportional to changes in foundation stiffnesses. Consequently, this paper explores the use of static stiffness measurements to determine the integrity of a foundation. However, the discussion in Section 3.3 warns that these benefits may be compromised by practical limitations on where and, in particular, how close to the foundation's elastic centre the static stiffness may be measured.

4.2. Identifying foundation stiffnesses from static response

In this section we consider the feasibility of inferring k_t and k_r from two point static stiffness measurements, i.e., when the sensor and force are collocated. Suppose that we measure the response per unit static input force at normalised distances h_1 and h_2 from the elastic centre and denote them by X_1/F and X_2/F. Then referring to Eqs. (20) and (22),

$$\frac{X_1}{F} = \frac{1}{k_t} + \frac{h_1^2}{k_r/l^2}, \quad \frac{X_2}{F} = \frac{1}{k_t} + \frac{h_2^2}{k_r/l^2}. \tag{24}$$

In matrix form

$$\begin{Bmatrix} \frac{X_1}{F} \\ \frac{X_2}{F} \end{Bmatrix} = \begin{bmatrix} 1 & h_1^2 \\ 1 & h_2^2 \end{bmatrix} \begin{Bmatrix} \frac{1}{k_t} \\ \frac{1}{k_r/l^2} \end{Bmatrix}, \tag{25}$$

where $1/k_t$ and $1/k_r/l^2$ are sought and the foundation depth l is assumed known.

Providing that the two measurements are taken at different positions ($h_1 \neq h_2$) then the matrix of measurement positions is non-singular and invertible, albeit potentially ill-conditioned. Therefore, we may invert Eq. (25) to obtain the equivalent spring constants:

$$\begin{Bmatrix} \frac{1}{k_t} \\ \frac{1}{k_r/l^2} \end{Bmatrix} = \begin{bmatrix} 1 & h_1^2 \\ 1 & h_2^2 \end{bmatrix}^{-1} \begin{Bmatrix} \frac{X_1}{F} \\ \frac{X_2}{F} \end{Bmatrix}. \tag{26}$$

The foundation profile constant p, can be calculated from the ratio of the two estimated quantities:

$$p = \frac{1/k_t}{1/(k_r/l^2)}. \tag{27}$$

This estimate of p can be expected to be lower than the theoretical upper bound of $\frac{1}{4}$ established in Section 3.2.2. The normalised rotational stiffness can then be calculated from $\gamma = p\hat{l}^2$.

It must be ensured that the matrix in Eq. (25) is not only invertible but also well conditioned. If poorly conditioned then the estimates for k_t and k_r may be severely corrupted in two ways:

(i) small measurement errors in the static stiffnesses will be amplified greatly in the inferred values for k_t and k_r, and
(ii) inaccuracies in the matrix itself will heavily bias the estimates for k_t and k_r. This can occur due to inaccuracies in identifying the exact measurement locations relative to the elastic centre, whose position is uncertain (inclusion of the elastic centre as an unknown parameter would result in a non-linear estimation problem which is beyond the scope of this paper).

The condition of the inverse problem can be determined by applying equal row weighting to Eq. (25) and then taking the ratio of the matrix's larger to smaller singular value. This condition number is presented here as a qualitative measure of how sensitive the stiffness estimates are to measurement noise. A value of unity indicates optimal conditioning.

In accordance with recommendations from Section 3.4 one would be well advised to choose one measurement at ground level ($h_1 = \frac{1}{2}$) to best observe the translational spring, and vary the location of the second measurement, h_2, so as to ensure that the inverse problem is well conditioned. The condition number of the resulting inverse problem as a function of h_2 is shown in Fig. 11. Also shown is the condition number when the lower of the two measurements is at one, two and three times the foundation depth above ground level (beam length permitting). It is apparent that, with one measurement at ground level, the problem is well conditioned providing that the second measurement is at least one foundation depth above ground level ($h > 1\frac{1}{2}$). There is little benefit to be gained from measuring beyond twice the foundation depth ($h > 2\frac{1}{2}$). The

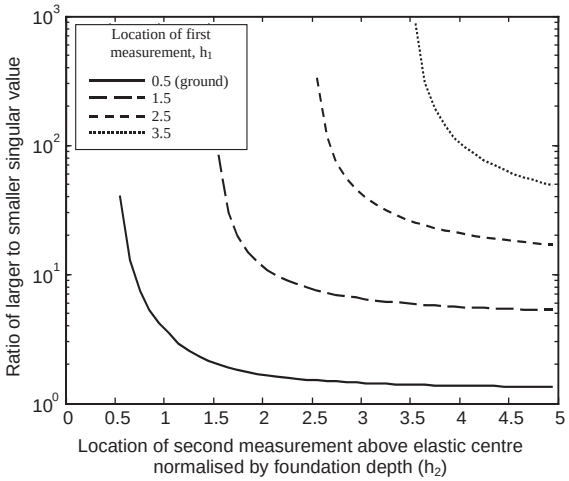

Fig. 11. Condition number of inverse problem to find rotational and translational spring constants from static stiffness measurements.

stiffness coefficients may still be estimated when the lower measurement is taken at one foundation depth above the ground. However, the lowest achievable condition number is increased by a factor of four or more, depending on the exposed length of the lamppost available for the second measurement. The stiffness estimates can be expected to be more susceptible to both measurement errors and the assumed location of the elastic centre. As the lower measurement is moved to two and three foundation depths above ground level then measurements of an order of magnitude more accurate are required in order to yield comparable stiffness estimates.

5. Experimental validation

5.1. Rig design

A rig was developed to represent a rigid beam constrained by discrete springs at distances 0 and l from one end. This arrangement represents the maximum ratio of rotational to translational stiffness, as described in Section 3.2.2. The rig comprised a stiff, massive frame to which the beam was hung from two discrete springs, as shown in Fig. 12. The beam was mounted upside-down to ensure static stability at low foundation depths. The springs took the form of two nominally identical short cantilevers whose bending stiffness was chosen such that the rigid body modes of the beam did not exceed 100 Hz. The fixed end of each cantilever was attached to a rigid shaft passing through a pair of journal bearings thereby eliminating the torsional stiffness of the cantilevers. One spring/shaft arrangement was fixed at one end of the beam and the other was moved along the length of the beam to vary the spring separation and hence the effective foundation depth.

Both the frame structure and the beam were required to behave rigidly in the frequency range of interest. The frame was designed using Finite Element analysis to ensure that its first

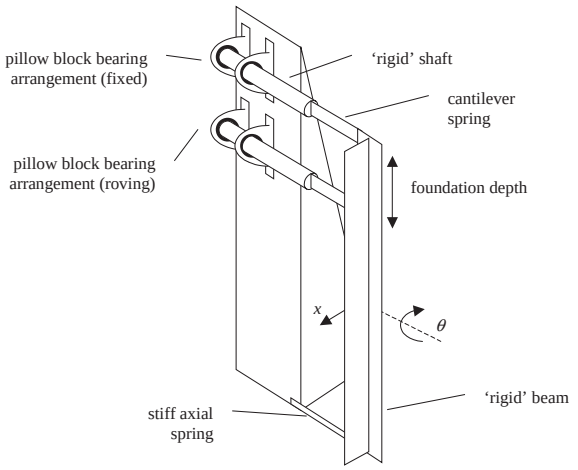

Fig. 12. Schematic of experimental rig of constrained rigid beam.

flexible mode was above 300 Hz. The beam was chosen to be a 600 mm long aluminium T-section with a first bending mode in the direction of excitation at about 250 Hz. In the lateral direction the beam is effectively clamped at 'ground level' resulting in an unacceptably low bending frequency for small foundation depths. This mode was shifted out of range by adding a third spring of high axial stiffness but very small bending and torsional stiffness at the otherwise free end of the beam.

5.2. Experimental procedure

Modal parameters and static stiffness values were deduced from appropriate frequency response function measurements obtained from tap tests.

To determine the natural frequencies, the beam was impacted at about 20% of its length from the constrained end to ensure excitation of both modes whilst avoiding excessive excitation and ringing of the lower frequency mode. The accelerometer was placed at the tip of the beam. The nodal points were determined by adjusting the impact location until each of the modes in turn was no longer excited. This procedure was repeated for foundation depths ranging from 5% to 100% of the beam length.

Static stiffness measurements were taken at a single foundation depth of 30%. Point FRF measurements were taken at a range of locations along the whole length of the beam including below ground level. Although unreachable in practical applications, the static stiffness measurement at the elastic centre ($\frac{1}{2}\hat{l}$) was particularly significant as a direct measure of the translational stiffness of the foundation.

Determining static stiffness values from dynamic measurements is not trivial due to poor signal to noise at low frequencies. A study into how this may be best achieved is beyond the scope of this paper. Instead, a single technique has been adopted here for the purposes of validating the theoretical model. Recall that the receptance between the jth and kth DOFs of a viscously damped

N degree of freedom system may be expressed as a modal summation:

$$\alpha_{j,k} = \sum_{i=1}^{N} \frac{\psi_{j,i}\psi_{k,i}}{(k_i - \omega^2 m_i) + \mathrm{i}(\omega c_i)}, \tag{28}$$

where k_i, m_i, c_i and $\{\psi\}_i$ are modal stiffness, mass, damping and displacements for the ith mode. Then the point static stiffness at the jth position along the beam may be deduced by equating j and k, setting ω to zero and truncating the series to include just the two rigid body beam modes. The static stiffness is given simply by

$$K_j = \sum_{i=1}^{2} \frac{k_i}{\psi_{j,i}^2}. \tag{29}$$

Conventional modal analysis techniques were used to extract the required modal parameters from the measured FRFs for substitution into Eq. (29).

5.3. Measured modal response

Fig. 13 shows the two measured natural frequencies of the beam as a function of foundation depth. An initial prediction is also shown as a dotted line. Notwithstanding the choice of linear axes, this prediction differs from that presented in Fig. 8 only in that the translational stiffness, k_t, of the rig is constant rather than proportional to foundation depth. Fig. 14 shows the nodal points of the two modes. The discrepancy between predicted and measured frequencies and mode shapes is stark. In Fig. 13, the rotational stiffness can be seen to rise much more steeply with foundation depth than predicted. This feature is a manifestation of the rig and is attributable to the rotational stiffness of the cantilever springs. When the beam moves rigidly the cantilevers deform due to forces applied at their free ends. Rotational motion of the beam requires the cantilevers to deform

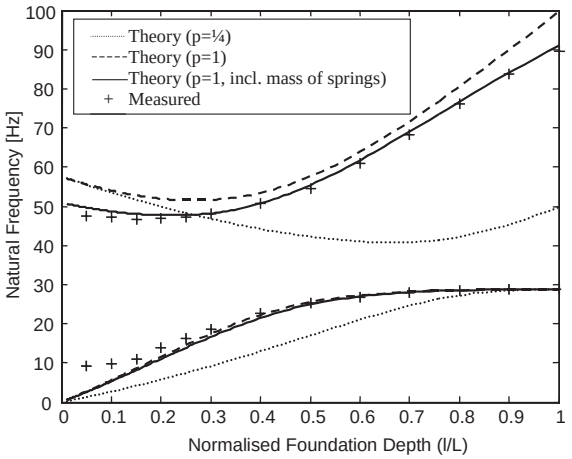

Fig. 13. Natural frequencies of rigid beam constrained by two discrete springs.

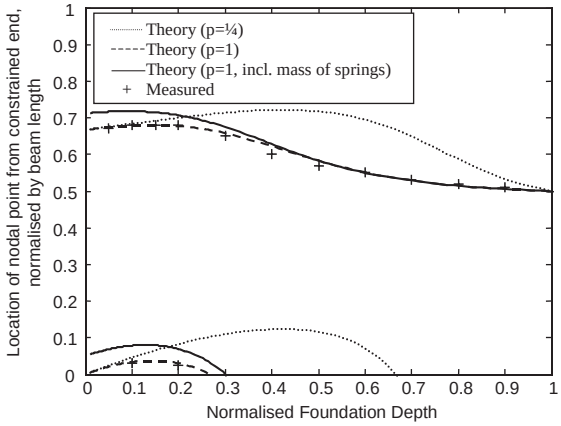

Fig. 14. Natural frequencies of rigid beam constrained by two discrete springs.

by differing amounts. If the beam were flexible in torsion then the two cantilever springs would be able to deform independently and assume different end slopes. However, since the beam is rigid in torsion then the beam applies a moment on the cantilever springs in order to constrain the springs to have the same end slope. Consequently, rotational motion of the rigid beam is also constrained by the rotational stiffness at the tips of the springs. It is shown in Appendix A that this effect increases the rotational stiffness from $\frac{1}{4}k_t\hat{l}^2$ to $k_t\hat{l}^2$. The effect is simulated in Figs. 13 and 14 by setting the foundation profile constant, p, to unity. The modes that are dominated by rotational stiffness are now closely predicted.

Two modest discrepancies remain in the prediction of the natural frequencies. The frequency of the second mode is over-estimated because the equivalent mass of the springs and associated fixings have been neglected. The effect of adding a 10 g lumped mass to each spring location is also shown in Figs. 13 and 14. The natural frequency is improved significantly although there is a modest deterioration in the prediction of the nodal points. The lower natural frequency is also under-predicted for shallow foundation depths ($\hat{l}<0.3$). This discrepancy can be attributed to the additional spring which was attached to the free end of the rigid beam. Although very flexible in bending its large moment arm contributed significantly to the rotational stiffness when the foundation springs were close together. Consequently, the third spring was replaced with one that was more flexible for the subsequent static stiffness tests presented in the following section.

5.4. Measured static response

Fig. 15 shows the measured static stiffness of the beam as a function of measurement position. Also shown is the static stiffness predicted by the model. A foundation profile parameter of unity has been chosen which accounts for the interaction effect of the springs, as discussed in Section 5.3. Despite some scatter arising from the indirect calculation procedure outlined in Section 5.2, the experiment provides adequate validation of the theoretical model. Note that the static stiffness peaks at about 15% of the beam's length which is the mid-depth of the foundation and hence the nominal position of the elastic centre.

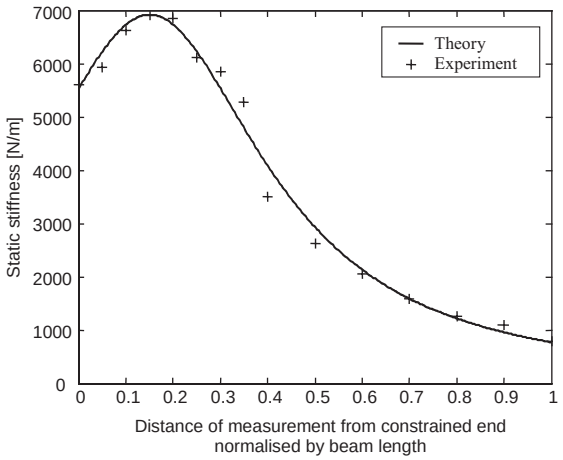

Fig. 15. Static stiffness of rigid beam constrained by two discrete springs.

5.5. Identification of foundation from static response

The static stiffness results presented in the previous section show that the translational stiffness of the rig's foundation, k_t, is about 7000 N/m, and that the rotational stiffness is given by $k_r = p\hat{l}^2 L^2 k_t$ where p is unity. However, in practice it is not possible to deduce k_t by measuring the static stiffness at the elastic centre of the foundation. This section demonstrates the procedure outlined in Section 4.2 for inferring the translational and rotational stiffnesses from two measurements taken above ground.

In Section 5.4, measured static stiffnesses were presented for 15 measurement locations along the beam. Only nine of these locations would be accessible in practice, including one at ground level. Of the many combinations of selecting two measurements from which to estimate the unknown stiffnesses only those combinations that included the ground-level measurement were investigated. Fig. 16 shows the estimated translational stiffness and foundation profile parameter when each of the other eight measurements was used in conjunction with the ground level measurement. When the second measurement is near the free end of the beam the estimated parameters are comparable to the known values. The discrepancy between the estimated and directly measured translational stiffness, for example, is about 10% which is of the same order of magnitude as the errors in the individual measurements (see Fig. 15). However, when the two measurements are closer together errors arise that are considerably larger than the errors in the individual measurements used in the estimation process. This is due to poor conditioning of the inverse problem as described in Section 4.2.

6. Concluding remarks

The dynamic and static response of a uniform rigid beam constrained at one end by an elastic foundation has been investigated. A simple model of the foundation has been adopted

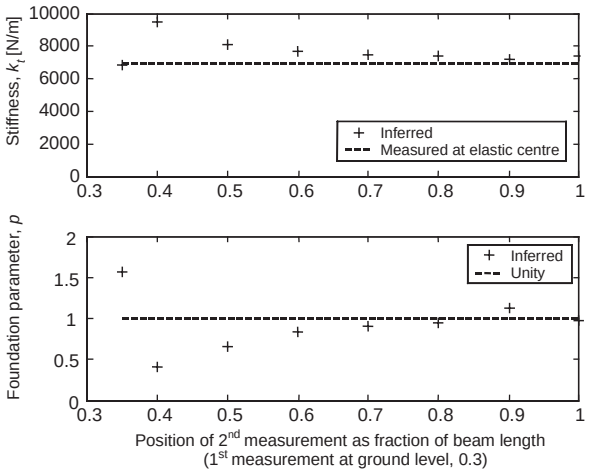

Fig. 16. Inferred translational stiffness, k_t, and foundation profile parameter, p, as a function of measurement location. Rotational stiffness, $k_r = p\hat{l}^2 k_t$ where $\hat{l} = 0.3$.

in order to establish a relationship between the rotational and translational stiffnesses. The rotational stiffness is proportional to the square of the foundation depth and the constant of proportionality is dependent on the foundation profile. A bound has been established for this constant, although experimental results emphasise that this bound is only valid when the foundation can be modelled by independently acting translational springs.

A modal analysis of the model has concluded that, unless the beam is predominantly buried, the two rigid body modes of the beam are well separated in frequency. The lower frequency mode is a pitching motion about a point close to its buried end and is controlled by the rotational stiffness of the foundation and the beam's inertia. The higher frequency mode is a pitching motion about a point around one-third of the beam's length from the free end and is controlled by the translational stiffness of the foundation and the mass of the beam. Neither natural frequency is very sensitive to changes in foundation stiffness.

The static stiffness, whilst more problematic to measure, is more sensitive to changes in foundation stiffness. Consequently, static stiffness measurements may be a suitable indicator of changes in the integrity of the foundation. A simple inverse technique has been presented by which the stiffnesses of the foundation in translation and rotation can be quantified from two point static stiffness measurements. The inverse problem is found to be well conditioned when the two measurements are well spaced, especially for shallow foundations. The technique has been successfully demonstrated on a laboratory rig.

Acknowledgements

The authors are grateful to the Royal Thai Embassy for their financial support.

Appendix A. Modelling spring interdependence

In the experimental rig, the beam is supported by two nominally identical cantilever springs of length L_s and stiffness $k = 3EI/L_s^3$, where E and I are the Young's modulus and second moment of area of the cantilevers respectively. These springs provide restoring forces of $F_1 = kx_1$ and $F_2 = kx_2$ where x_1 and x_2 are the deflections at the tips of the cantilevers, as shown in Fig. 17.

When the beam pitches, then $x_1 \neq x_2$ which requires the springs to assume different end slopes. However, if the beam spanning the springs is rigid in torsion then the condition $\phi_1 = \phi_2$ is enforced by the beam applying equal and opposite moments M_1 and M_2 to the ends of the springs. Consequently, the deflection of the springs due to these moments must be included in the equations of motion.

The spring forces and moments are related to the spring tip deflections by the following equations:

$$\begin{Bmatrix} x_1 \\ \phi_1 \end{Bmatrix} = \mathbf{A}_s \begin{Bmatrix} F_1 \\ M_1 \end{Bmatrix}, \quad \begin{Bmatrix} x_2 \\ \phi_2 \end{Bmatrix} = \mathbf{A}_s \begin{Bmatrix} F_2 \\ M_2 \end{Bmatrix}, \tag{A.1}$$

where $\mathbf{A}_s$ is a flexibility matrix given by

$$\mathbf{A}_s = \begin{bmatrix} \dfrac{L_s^3}{3EI} & \dfrac{L_s^2}{2EI} \\ \dfrac{L_s^2}{2EI} & \dfrac{L_s}{EI} \end{bmatrix}. \tag{A.2}$$

Inverting the flexibility matrix, and recalling that the combined translational stiffness of the two springs, k_t, is twice $3EI/L_s^3$, then the stiffness matrix may be written as

$$\mathbf{K}_s = k_t \begin{bmatrix} 2 & -L_s \\ -L_s & \frac{2}{3}L_s^2 \end{bmatrix}. \tag{A.3}$$

Eq. (A.1) can be rewritten as

$$\begin{Bmatrix} F_1 \\ M_1 \end{Bmatrix} = \mathbf{K}_s \begin{Bmatrix} x_1 \\ \phi_1 \end{Bmatrix}, \quad \begin{Bmatrix} F_2 \\ M_2 \end{Bmatrix} = \mathbf{K}_s \begin{Bmatrix} x_2 \\ \phi_2 \end{Bmatrix}. \tag{A.4}$$

Applying the following two constraints:

$$\phi_1 = \phi_2, \quad M_1 = -M_2 \tag{A.5}$$

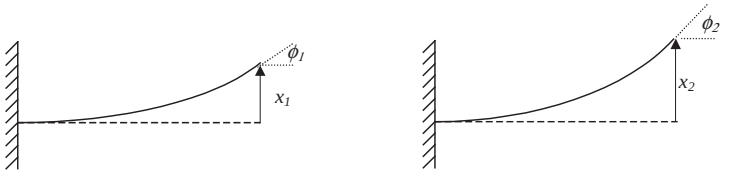

Fig. 17. Tip deflections of cantilever springs.

Eq. (A.4) can be simplified to give

$$\begin{Bmatrix} F_1 \\ M_1 \end{Bmatrix} = \mathbf{K}_s \begin{Bmatrix} x_1 \\ \phi_1 \end{Bmatrix}, \quad \begin{Bmatrix} F_2 \\ -M_1 \end{Bmatrix} = \mathbf{K}_s \begin{Bmatrix} x_2 \\ \phi_1 \end{Bmatrix}. \tag{A.6}$$

Adding the second rows together and rearranging gives the end slope of both springs

$$\phi_1 = \phi_2 = \frac{3}{4L_s}(x_1 + x_2). \tag{A.7}$$

The strain energy is given by

$$V = \{x_1 \quad \phi_1\}\mathbf{K}_s \begin{Bmatrix} x_1 \\ \phi_1 \end{Bmatrix} + \{x_2 \quad \phi_2\}\mathbf{K}_s \begin{Bmatrix} x_2 \\ \phi_2 \end{Bmatrix}. \tag{A.8}$$

Substituting for $\mathbf{K}_s$ from Eq. (A.3), and ϕ_1, ϕ_2 from Eq. (A.7) gives

$$V = \tfrac{1}{2}k_t(2x_1^2 + 2x_1^2 - \tfrac{3}{4}(x_1 + x_2)^2). \tag{A.9}$$

The deflections of the two springs can be related to the state variables, x and $L\theta$, as follows:

$$x_1 = x - \tfrac{1}{2}L\theta, \quad x_2 = x - (\tfrac{1}{2} - \hat{l})L\theta. \tag{A.10}$$

Substituting for x_1 and x_2 from Eq. (A.10) into Eq. (A.9) gives

$$V = \tfrac{1}{2}k_t(2(x - \tfrac{1}{2}L\theta)^2 + 2(x - (\tfrac{1}{2} - \hat{l})L\theta)^2 - \tfrac{3}{4}(2x - (1 - \hat{l})L\theta)^2). \tag{A.11}$$

Using Lagrange's equation the stiffness matrix can be derived:

$$\mathbf{K} = k_t \begin{bmatrix} 1 & -\tfrac{1}{2}(1 - \hat{l}) \\ -\tfrac{1}{2}(1 - \hat{l}) & \tfrac{1}{4}(1 - \hat{l})^2 + \hat{l}^2 \end{bmatrix}. \tag{A.12}$$

By comparing Eq. (A.12) with Eq. (19) it is apparent that the effect of constraining the end slopes of the cantilever springs to be equal is to increase the normalised rotational stiffness, γ, from $\frac{1}{4}\hat{l}^2$ to $\hat{l}^2$.

Appendix B. Nomenclature

α	receptance
β	geometric mean of sensor and force locations/beam length
γ	normalised rotational stiffness
θ	deflection of rotational spring
ψ	modal displacements
a	ratio of discrete spring stiffnesses
c_i	modal damping
F	force
$h,\ h_1,\ h_2$	geometric mean of sensor and force locations/foundation depth
K	static stiffness
$\mathbf{K}$, $\mathbf{M}$	stiffness and mass matrices
k_1, k_2	discrete spring stiffnesses
k_i	modal stiffness

k_r	rotational stiffness
k_t	translational stiffness
l	foundation depth
L	beam length
$\hat{l}$	foundation depth normalised by beam length
l_s, l_f	sensor and force locations
m	beam mass
m_i	modal mass
p	foundation profile constant
$w(z)$	spring stiffness per unit foundation depth
x	deflection of translational spring
X_s, X_e, X_1, X_2	translational displacements
z	height from constrained end of beam
z_e	location of elastic centre

References

[1] L. Hibbert, Throwing light on a hidden menace, *Professional Engineering* 11 (3) (1998) 22.
[2] P. Cawley, R.D. Adams, The location of defects in structures from measurements of natural frequencies, *Journal of Strain Analysis* 14 (2) (1979) 49–57.
[3] G. Hearn, R.B. Testa, Modal analysis for damage detection in structures, *Journal of Structural Engineering* 117 (10) (1991) 3042–3063.
[4] S.W. Doebling, F.M. Hemez, L.D. Peterson, C. Farhat, Improved damage detection accuracy using strain energy based mode selection criteria, *American Institute of Aeronautics and Astronautics Journal* 35 (4) (1997) 693–699.
[5] C.P. Ratcliffe, Damage detection using a modified Laplacian operator on mode shape data, *Journal of Sound and Vibration* 204 (3) (1997) 505–517.
[6] H.A. Razak, F.C. Choi, The effect of corrosion on the natural frequency and modal damping of reinforced concrete beams, *Engineering Structures* 23 (9) (2001) 1126–1133.
[7] S. Alampalli, G. Fu, E.W. Dillon, Signal versus noise in damage detection by experimental modal analysis, *Journal of Structural Engineering* 123 (2) (1997) 237–245.
[8] S. Alampalli, Effects of testing, analysis, damage, and environment on modal parameters, *Mechanical Systems and Signal Processing* 14 (1) (2000) 63–74.
[9] B. Peeters, J. Maeck, G. De Roeck, Vibration-based damage detection in civil engineering: excitation sources and temperature effects, *Smart Materials and Structures* 10 (3) (2001) 518–527.
[10] D.M. McCann, M.C. Forde, Review of NDT methods in the assessment of concrete and masonry structures, *NDT&E International* 34 (2) (2001) 71–84.
[11] S.W. Doebling, C.R. Farrar, M.B. Prime, A summary review of vibration-based damage identification methods, *Shock and Vibration Digest* 30 (2) (1998) 91–105.
[12] C.R. Farrar, S.W. Doebling, D.A. Nix, Vibration-based structural damage identification, *Philosophical Transactions of the Royal Society A* 359 (1778) (2001) 131–149.
[13] D.J. Pines, Detection of utility pole damage by measuring the reflection coefficient, *Journal of Nondestructive Evaluation* 16 (1) (1997) 43–56.
[14] J. Axmon, M. Hansson, L. Sörnmo, Modal analysis of living spruce using a combined prony and DFT multichannel method for detection of internal decay, *Mechanical Systems and Signal Processing* 16 (4) (2002) 561–584.

[15] D. Ouis, Vibrational and acoustical experiments on logs of spruce, *Wood Science and Technology* 33 (1999) 151–184.
[16] F.K. Choy, R. Liang, P. Xu, Fault identification of beams on elastic foundation, *Computers and Geotechnics* 17 (2) (1995) 157–176.
[17] A.S. Purekar, D.J. Pines, Detecting damage in non-uniform beams using the dereverberated transfer function response, *Smart Materials and Structures* 9 (4) (2000) 429–444.